

Experimentally-determined characteristics of radiant systems for office buildings

Hongyuan Jia^{a,b,c}, Xiufeng Pang^{c,*}, Philip Haves^c

^a Key Laboratory of Three Gorges Reservoir Region's Eco-Environment, Ministry of Education, Chongqing University, Chongqing 400045, China

^b National Center for International Research of Low-carbon and Green Buildings, Chongqing University, Chongqing 400045, China

^c Lawrence Berkeley National Laboratory, Berkeley, CA 94720, USA

HIGHLIGHTS

- In radiant ceiling panel system, the temperature stratification is modest in cooling mode.
- Air temperature can be used in lieu of operative temperature in controlling radiant systems.
- Use of thin carpet requires the chilled water temperature to be reduced by ~1 K in radiant slab system.

ARTICLE INFO

Keywords:

Radiant systems
Stratification
Operative temperature
Variation in comfort
FLEXLAB

ABSTRACT

Radiant heating and cooling systems have significant energy-saving potential and are gaining popularity in commercial buildings. The main aim of the experimental study reported here was to characterize the behavior of radiant cooling systems in a typical office environment, including the effect of ceiling fans on stratification, the variation in comfort conditions from perimeter to core, control on operative temperature vs. air temperature and the effect of carpet on cooling capacity. The goal was to limit both the first cost and the perceived risk associated with such systems. Two types of radiant systems, the radiant ceiling panel (RCP) system and the radiant slab (RS) system, were investigated. The experiments were carried out in one of the test cells that constitute the FLEXLAB test facility at the Lawrence Berkeley National Laboratory in March and April 2016. In total, ten test cases (five for RCP and five for RS) were performed, covering a range of operational conditions. In cooling mode, the air temperature stratification is relatively small in the RCP, with a maximum value of 1.6 K. The observed stratification effect was significantly greater in the RS, twice as much as that in the RCP. The maximum increase in dry bulb temperature in the perimeter zone due to solar radiation was 1.2 K for RCP and 0.9 K for RS – too small to have a significant impact on thermal comfort. The use of ceiling fans was able to reduce any excess stratification and provide better indoor comfort, if required. The use of thin carpet requires a 1 K lower supply chilled water temperature to compensate for the added thermal resistance, somewhat reducing the opportunities for water-side free cooling and increasing the risk of condensation. In both systems, the difference between the room operative temperature and the room air temperature is small when the cooling loads are met by the radiant systems. This makes it possible to use the air temperature to control the radiant systems in lieu of the operative temperature, reducing both first cost and maintenance costs.

1. Introduction

Radiant heating and cooling systems are increasing in popularity in both residential and commercial applications [1,2]. One of their advantages is that heat is supplied or extracted through direct radiative heat transfer between the human body and radiant surfaces, as well as indirectly, through convection [3], enabling a radiant cooling system to provide thermal comfort at a higher room air temperature. Radiant

cooling systems use higher supply temperatures than mixing ventilation forced air systems and so can make more use of water-side free cooling. Hydronic systems also reduce fan power by more than their increased pump power, which also reduces system energy consumption.

According to ISO 11,855 [4], radiant systems are categorized into three main types: radiant ceiling panels (RCP), embedded surface systems (ESS) and thermally activated building systems (TABS). The TABS and some ESSs have the ability to smooth and shift peak HVAC loads

* Corresponding author at: One Cyclotron Road, MS 90R3147, Berkeley, CA 94720, USA.
E-mail address: xpang@lbl.gov (X. Pang).

Nomenclature	
Variables	
σ	Stefan-Boltzmann constant ($\text{W}\cdot\text{m}^{-2}\cdot\text{K}^4$)
D	diameter of globe temperature sensor (m)
ΔT_a	air temperature difference at two different heights (K)
ϵ_g	emissivity of the globe temperature sensor
h_c	convective heat transfer coefficient ($\text{W}/(\text{m}^2\cdot\text{K})$)
Q	chilled water flow rate (L/s)
Q_{solar}	solar irradiance (W/m^2)
RH	relative humidity (%)
T_a	air dry-bulb temperature (°C)
T_g	globe temperature (°C)
T_{op}	operative temperature (°C)
T_r	mean radiant temperature (°C)
$T_{w,sup}$	chilled water supply temperature (°C)
v	air speed (m/s)
Subscripts	
a, h	air at h m height
ave	average
oa	outdoor air

and are primarily applied in new constructions, although pipes embedded in a relatively thin topping slab can be installed on the structural slab in some existing building applications [5,6]. RCPs can be installed in suspended ceilings, and so are relatively easy to retrofit in existing buildings, but have no thermal storage capability.

Radiant systems have been widely studied in the literature [7,8]. Rhee and Kim [7] conducted a comprehensive review of the basic and applied research on radiant heating and cooling systems in terms of thermal comfort, energy performance, system configuration and control strategies over the last 50 years. They concluded that radiant heating and cooling systems are fully understood on the basis of building physics and engineering technology, and the future studies should focus on overcoming the limitations and barriers in their application to broader building types and climates. These barriers include the challenge of achieving effective control of radiant slabs due to their long response times. Karmann et al. [8] conducted a critical review of thermal comfort in buildings using radiant systems compared to all-air systems. They concluded that there are indications that radiant systems can provide equal or better comfort than all-air systems.

Recently, some reports in the literature have focused on the differences of sensible zone cooling loads between air system and radiant system [9–12]. Bauman et al. [10] discuss the need for both a new definition of radiant system zone cooling load and the development of a new load calculation procedure.

Table 1 gives a summary of stratification effect values in radiant systems reported in the literature. Causone et al. [13] reported that thermal stratification between 1.1 m and 1.7 m was found with an average value of 0.6 K in cooling mode and 1.1 K to 1.8 K in heating mode. Immanri et al. [14] compared the thermal comfort and energy consumption of a RCP, an air handling unit (AHU) and combined RCP with AHU serving a conference room, concluding that in heating mode the combined system produces smaller stratification of room air temperature, with a max value of 0.9 K between 0.1 m and 1.1 m, and is able to generate a more comfortable environment than the AHU running alone. Song et al. [15] examined a RS system integrated with a dedicated outside air system (DOAS) with outdoor reset control. An air temperature stratification of approximately 2.0 K between 0.1 m and

1.1 m was observed when the indoor temperature was regulated at 26 °C. Causone et al. [16] conducted laboratory experiments showing that under a typical European office room layout, RS system combined with displacement ventilation (DV) could create modest air stratification (0.4–0.9 K) between head and ankles, but may cause thermal discomfort when running in cooling mode with a maximum difference value of 6.6 K. Schiavon et al. [17] investigated the effect of the ratio of cooling load removed by a RCP integrated with DV, and concluded that the air stratification effect was highly influenced by the portion of cooling load removed by the RCP and the surface temperature of the cooled radiant panel. Zhao et al. [18] proposed a radiant-capillary-terminal (RCT) floor heating system with solar phase change thermal storage (SPCTS). The vertical temperature differences from 0.1 m to 1.1 m above the floor ranged from 0.6 K to 0.9 K in their study. However, some of the above mentioned experiments [13,17] were conducted in test chambers that have no windows and so the impact of the solar heat gains was not considered in their studies.

The temperature of a radiantly-conditioned space is generally evaluated in terms of the operative temperature, which is defined as the weighted average of air temperature and mean radiant temperature and is often used as an index to evaluate thermal comfort and size radiant heating and cooling systems [19]. ISO 7726 [20] lists three methods for measuring the mean radiant temperature, i.e., (1) using black-globe thermometer, which is the most commonly used one [21], (2) using two sphere radiometer, (3) using constant air temperature sensor. For the HVAC (heating, ventilation and air-conditioning) applications, both ISO [20] and ASHRAE [21] recommend a black-globe thermometer consists of a hollow sphere of 150 mm diameter, coated in flat black paint with a thermocouple or thermometer bulb at its center, with a response time of 20–30 min. However, because of its size and the long-time constant characteristic, it is impractical to use it in the control of HVAC systems [22]. It is possible to use a smaller globe, thought the change in size increases the weighting of the air temperature relative to the radiant temperature; however, it has recently been suggested [23] that the difference between the air temperature and the operative temperature in radiantly-cooled commercial spaces may be small enough to allow the air temperature to be used as a proxy for the operative temperature.

Table 1
Summary of ranges of thermal stratification of radiant cooling systems in previous studies.

Reference	System	Test facility	Floor area (m ²)	Height range (m)	Temperature stratification (K)
Causone et al. [13]	RCP	Underground test chamber	11.6	1.1–1.7	0.6 (Cooling mode) 1.1–1.8 (Heating mode)
Immanri et al. [14]	RCP + AHU	Small office meeting room	33.0	0.1–1.1	0.9 (Heating mode)
Song et al. [15]	RS + DOAS	Thermally insulated test cell	5.8	0.1–1.1	2.0 (Cooling mode)
Causone et al. [16]	RS + DV	Thermally insulated test cell	16.8	0.1–1.1	3.2–6.6 (Cooling mode) 0.4–0.9 (Heating mode)
Schiavon et al. [17]	RCP + DV	Test chamber within a large conditioned test hall	18.2	0.1–1.1	1.5 or higher when all radiant ceiling surface temperatures are 18 °C or higher (Cooling mode)
Zhao et al. [18]	RCT + SPCTS	One room of a residential house	11.8	0.1–1.1	0.6–0.9 (heating mode)

Since the temperature control of occupied spaces conventionally uses air temperature sensors which are easier and less expensive to manufacture and install than operative temperature sensors, there is a need to investigate whether air temperature can be used in lieu of operative temperature as the feedback control variable for radiant systems.

In perimeter spaces, direct solar heat gain constitutes a large portion of cooling load, and has significant impact on both thermal comfort and energy consumption. Research efforts have been made to understand thermal environment variations between perimeter spaces and core spaces, as well as design strategies to balance daylighting harvesting and cooling load reduction. Bessoudo et al. [24] performed an experimental study of indoor thermal conditions near glazed façades with shading devices, showing that in winter, even on very cold ($< -15^{\circ}\text{C}$) sunny days, the operative temperature at the head level of seated occupants 1.5 m from an unshaded window could reach 31°C when the total incident solar radiation was greater than 800 W/m^2 , causing substantial thermal discomfort. They concluded that, in a cold climate, perimeter heating could be eliminated when using a double glazed, low-e window with a roller shade [25]. Gan [26] analyzed the effect of glazing on indoor thermal comfort in an office in heating mode using numerical modeling and found that thermal discomfort may result from the combination of radiant heating panels and a large single-glazed window in a cold climate, due to radiant asymmetry. As regards cooling, Tzempelikos and Athienitis [27] presented a simulation-based analysis of the impact of glazing and shading control on cooling and lighting energy for perimeter office spaces in Montreal. They concluded that 30% window-to-wall ratio could ensure sufficient natural daylight for 76% of the year and also suggested that cooling was still needed for perimeter office spaces with high solar gains, even in heating-dominated climates. Feng [28] conducted surveys and interviews of twelve leading practitioners and manufacturers in U.S., investigating radiant

system design approaches used in practice. The results showed that there was confusion and uncertainty when designing radiant systems with high solar radiation. Overall, there is still a lack of full-scale experimental investigation of the thermal comfort variations from perimeter to core in radiant cooling systems and the possible need to implement separate system control for perimeter areas near windows.

In general, radiant systems are installed in or on large surfaces; keeping these surfaces exposed can be difficult when integrating acoustical absorbents [8]. In practice, concrete surfaces used in RS systems are often left uncovered [29]. However, the impact of floor coverings on the performance of radiant systems is not well addressed in the literature. Some numerical analyses [30,31] and experimental studies [32,33] had been conducted to illustrate the heat transfer between radiant systems and the indoor environment. Zhao et al. [34] compared the sheltered (by furniture) and unsheltered radiant floors in large space buildings, e.g. airports and railway stations. They found that the sheltered radiant floor had much lower surface temperature, usually $3.8\text{--}7.5\text{ K}$, than the unsheltered radiant floor, and thus has higher risk of condensation.

The purpose of this study was to conduct full-scale laboratory experiments for both RCP and RS systems in a typical U.S. office configuration to provide information for researchers and practitioners on aspects of radiant system performance that have received relatively little attention in the literature but relate to first cost and perceived performance risks associated with radiant heating and cooling systems. These include (1) stratification and the effect of ceiling fans, (2) variation in comfort from perimeter to core, (3) control based on operative temperature vs. air temperature and (4) effect of carpet on cooling capacity. The aim of the study was to improve the energy and comfort performance of commercial buildings by encouraging the appropriate adoption of radiant systems in various building types and climates.

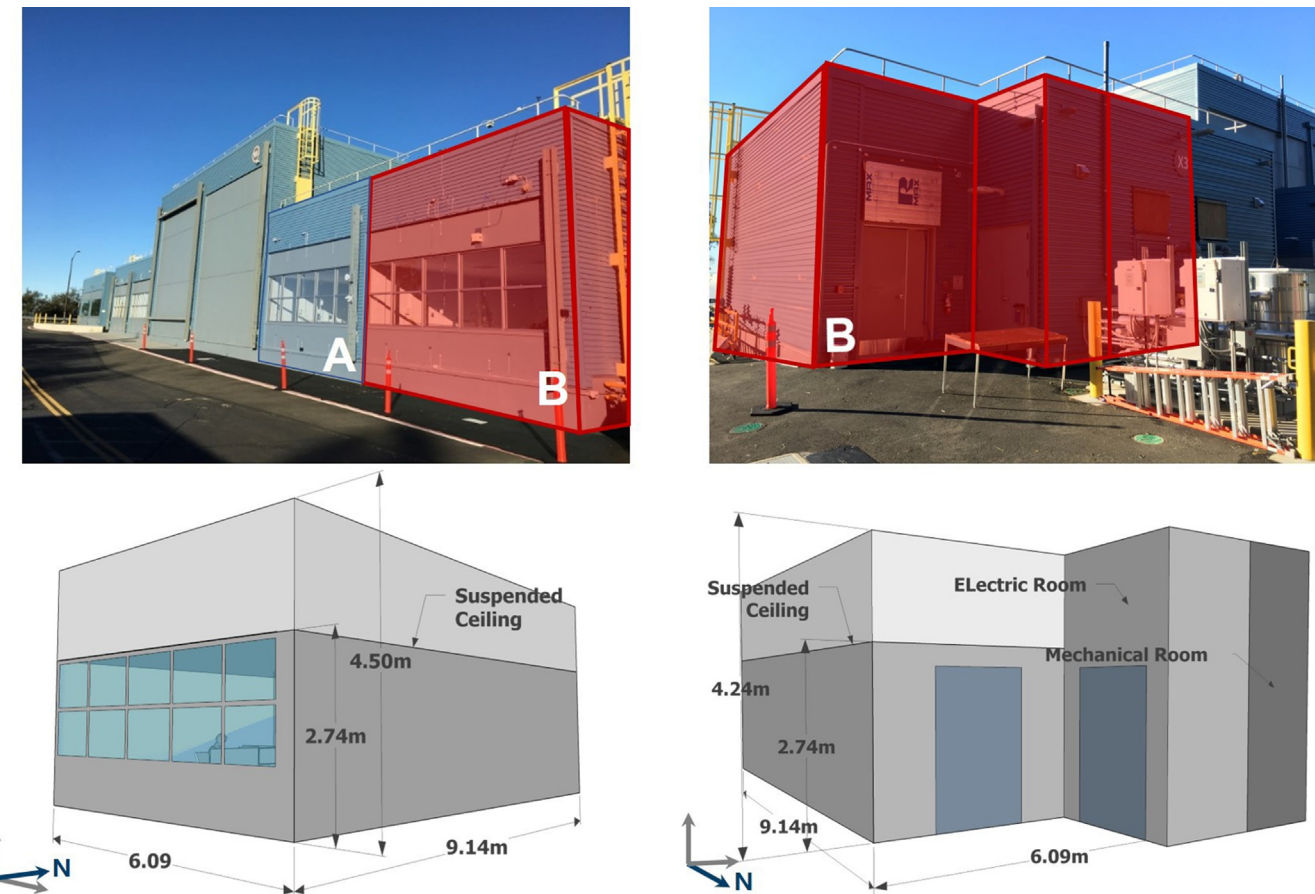


Fig. 1. FLEXLAB at LBNL.

2. Methodology

2.1. Experiment facility

This study reported here was performed in the Facility for Low Energy eXperiments (FLEXLAB [35]) at the Lawrence Berkeley National Laboratory (LBNL). FLEXLAB has four test beds designed to simulate real-world conditions of energy efficiency interventions, as shown in Fig. 1. Each test bed consists of two side-by-side cells with the same dimensions. The thermal isolation resulting from the near adiabatic walls between adjacent cells allows their performance to be analyzed independently. The test experiments were carried out in one cell (marked as B in Fig. 1) of one test bed (which consists of two cells, marked A and B in Fig. 1). Each cell has a floor area of 55.7 m^2 ($9.14 \text{ m} \times 6.09 \text{ m}$) with a roof height of 4.50 m (South) and 4.24 m (North). There is a suspended T-bar ceiling placed at a height of 2.74 m above the floor that supports either the radiant panels in the RCP system or conventional fiber-board ceiling tiles, in each case covered with 100 mm of polyisocyanurate insulation.

The south facade was configured with two rows of five windows, each with two clear panes and a low emissivity coating, above a conventional stud wall with a heat transmission coefficient of $0.46 \text{ W}/(\text{m}^2\text{K})$, configured to comply with the prescriptive requirements of the California Title 24 building energy code [36]. The east façade has a heat transmission coefficient of $0.07 \text{ W}/(\text{m}^2\text{K})$ and the partition wall between Cell B and Cell A, which bounds the west side of Cell B, has a heat transmission coefficient of $0.16 \text{ W}/(\text{m}^2\text{K})$. The mechanical room and electrical room are located on the north side of the cell and provide a thermal buffer for $\sim 60\%$ of the north wall, the remainder of which has a heat transmission coefficient of $0.56 \text{ W}/(\text{m}^2\text{K})$.

In order to simulate more realistic office conditions, six simulated work spaces consisting of thermal manikins, computers, desks and partitions were set up, together with ceiling fans and artificial lights, as shown in Fig. 2. The manikins were wound with heating tape and the supply voltages were adjusted to produce a sensible heat dissipation rate of about 80 W each, corresponding to the metabolic rate of sedentary office works in a low humidity environment. The advantage of the thermal manikins is that their radiative/convective splits, and the characteristics of their thermal plumes, are more realistic than the heated cylinders specified in EN 14240 [37]. LCD screens, lights and manikins were activated on a typical office schedule, and the power consumption of the computers was managed using a script running on each computer that varied the computational load to follow a pre-defined profile. The power consumptions of all the internal heat loads were carefully measured and summarized in Table 2. The total power density is $\sim 29 \text{ W/m}^2$. The measured solar gain on a clear day in the middle of the test period was 77 W/m^2 at solar noon and 39 W/m^2 averaged over the period 6:00–18:00. Three ceiling fans were installed in order to investigate their influence on air speed and stratification and on convective heat transfer at the surfaces of the slab and the radiant panels. The air speed at desk height directly below the fans was 1.1 m/s at speed Level 2 and 1.5 m/s at speed Level 3.

The test cell has both the RCP system and the RS system installed. As shown in Fig. 3, hot and chilled water were supplied by a dedicated boiler and a dedicated chiller, each equipped with a buffer tank to reduce the supply temperature fluctuations due to boiler or chiller cycling. Hot water or chilled water could be selected using automatic control valves. The inlet water temperature to the radiant system was varied by mixing supply water from the boiler or the chiller with return water from the radiant system. The flow rate in each sub-zone was controlled independently by modulating a control valve. In this study, each sub-zone has the same inlet water temperature. The ventilation system was not used in this study.

2.1.1. Configuration of the RCP system

72 radiant panels were mounted in the existing T-bar ceiling at a

height of 2.7 m above the floor. Each panel is $609.6 \text{ mm} \times 609.6 \text{ mm}$ and consists of 12.7 mm diameter copper pipe connected thermally to the back of a sheet of aluminum and is covered by foil-faced batt insulation, as shown in Fig. 4. The panels were connected together at the back by push-on flexible hoses. The panels are a commercial product that has been in use for a number of years. The panels occupied 51% of the entire ceiling area, with the remaining area covered with conventional ceiling tiles. The radiant system was divided into three sub-zones, and each sub-zone had two circuits of panels connected in series, as shown in the left chart in Fig. 5. The radiant panels were painted to match the optical reflectivity of the conventional ceiling tiles, so as not to affect the daylighting performance. Some of the panels have six passes of the copper pipe, increasing their capacity compared to the remaining panels, which have four; a higher proportion of four pass panels were installed in Zone 3, which has a larger area, in order to balance the loads on each circuit. Zone 3 is furthest from the window and so was subject to lower solar heat loads.

2.1.2. Configuration of the RS system

The RS system was separated into three zones, each containing multiple circuits of PEX tubing, and with floor areas of 19.6 m^2 , 15.3 m^2 , and 23.0 m^2 , as shown in Fig. 5. The nominal diameter of the tubing is 16 mm and the internal diameter is 12.7 mm. The schematic diagram of the slab construction is shown in Fig. 6. According to ISO 11855-2 [4], the tested RS system was categorized into Type C of the ESS.

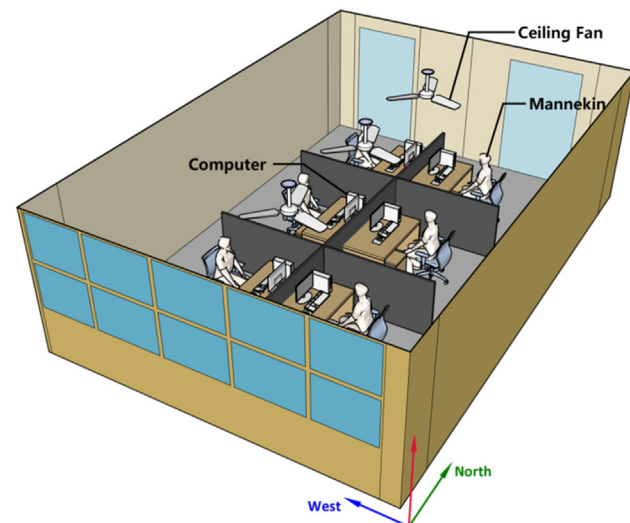


Fig. 2. Test cell setup.

Table 2
Internal loads summary.

Internal load type	Number	Schedule	Peak power (W)	Power density (W/m ²)
Computers	6	08:00–18:00	532	9.53
Manikins	6	07:00–19:00	499	8.95
Lights	6	00:00–24:00 (Case 1–3) 07:00–19:00 (Case 4–10)	279	5.00
Sensing devices and data acquisition	N/A	00:00–24:00	65	1.16
Circulation pump	1	00:00–24:00	215	3.86
Total	N/A	N/A	1590	28.51

2.2. Instrumentation

Fifty-eight temperature sensors were used to measure the surface temperatures of the walls, windows, floor and ceiling with every surface having at least six temperature sensors as shown in Fig. 7. Three vertical arrays of temperature sensors (Tree 1, Tree 2 and Tree 3 in Fig. 7), fixed at seven different heights, were used to calculate the mean air temperature and observe the air temperature stratification, as shown in Fig. 8 (left). The heights of the temperature sensors on the vertical ‘trees’ followed ANSI/ASHRAE Standard 55-2013 [38], as shown in Table 3. Each air temperature sensor was surrounded by a radiation shield, painted white to reflect solar radiation according to EN 14,240 [37], as shown in Fig. 8 (upper right). An air speed sensor was placed on the desk at the center of the test cell, at a height of 0.76 m above the floor to measure the air speed produced by the ceiling fans.

Since the globe temperature was an input to the calculation of operative temperature, which was used for zone temperature control

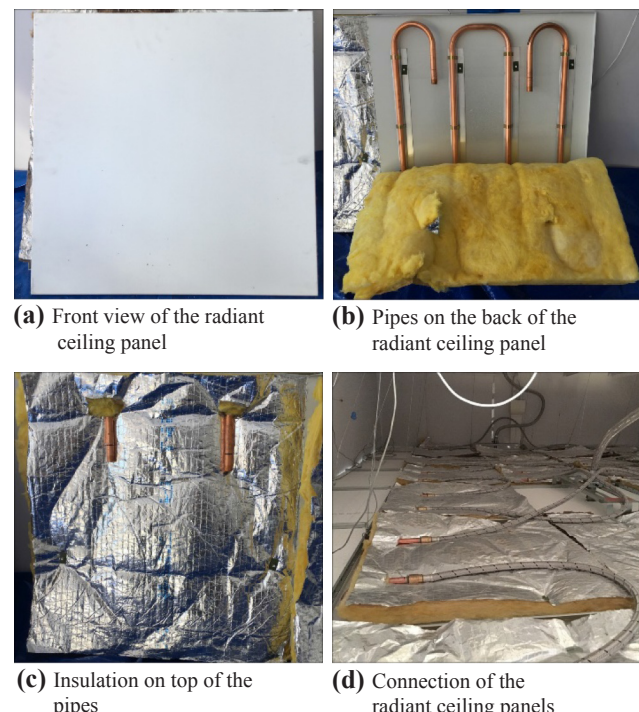


Fig. 4. The radiant ceiling panel.

during some of the tests, a quick response globe temperature sensor was required. The response time of a 150 mm diameter globe thermometer, as specified in ISO 7726 [20], is ~20 to 30 min, which was considered to be too long for these tests. Three smaller globe thermometers were

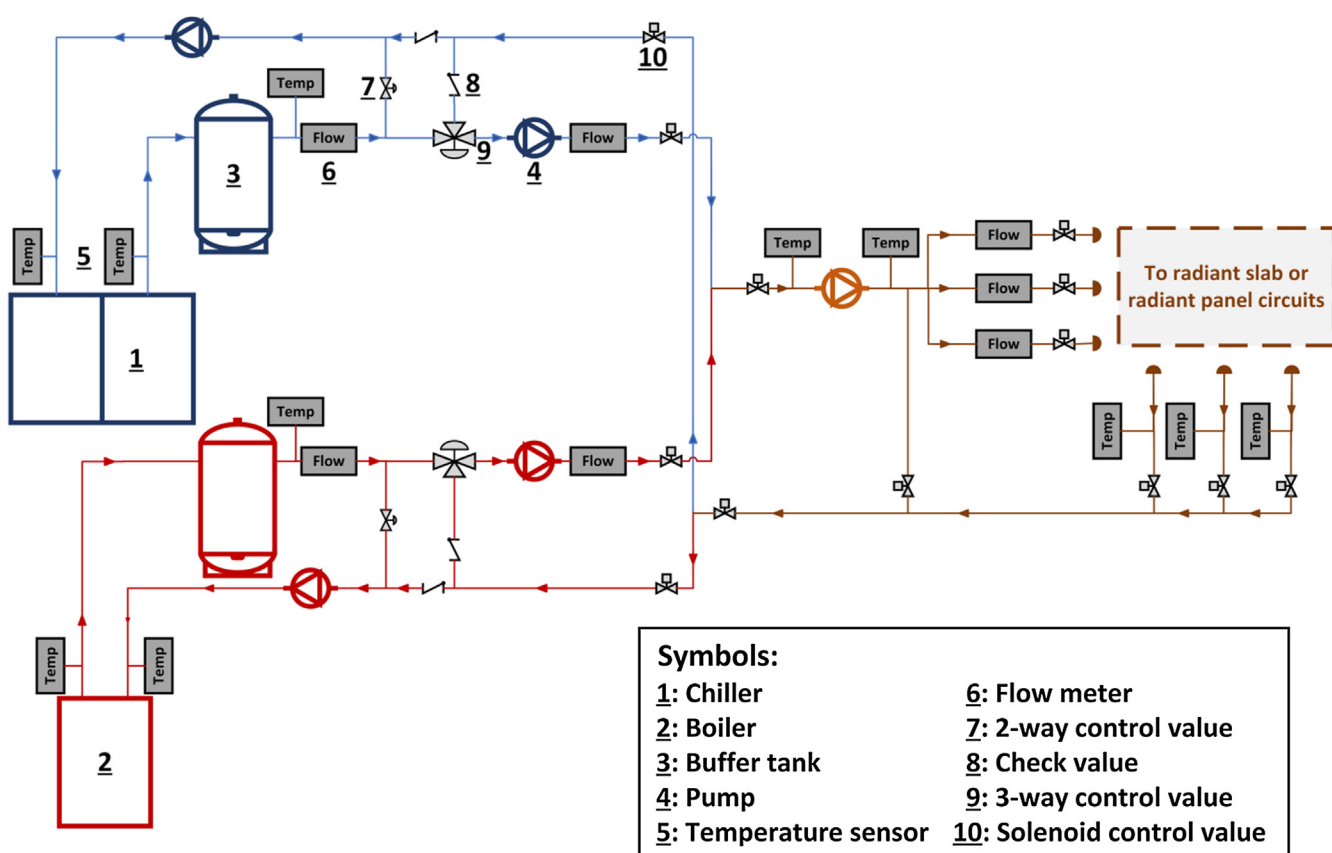


Fig. 3. Schematic diagram for the chilled and hot water plant.

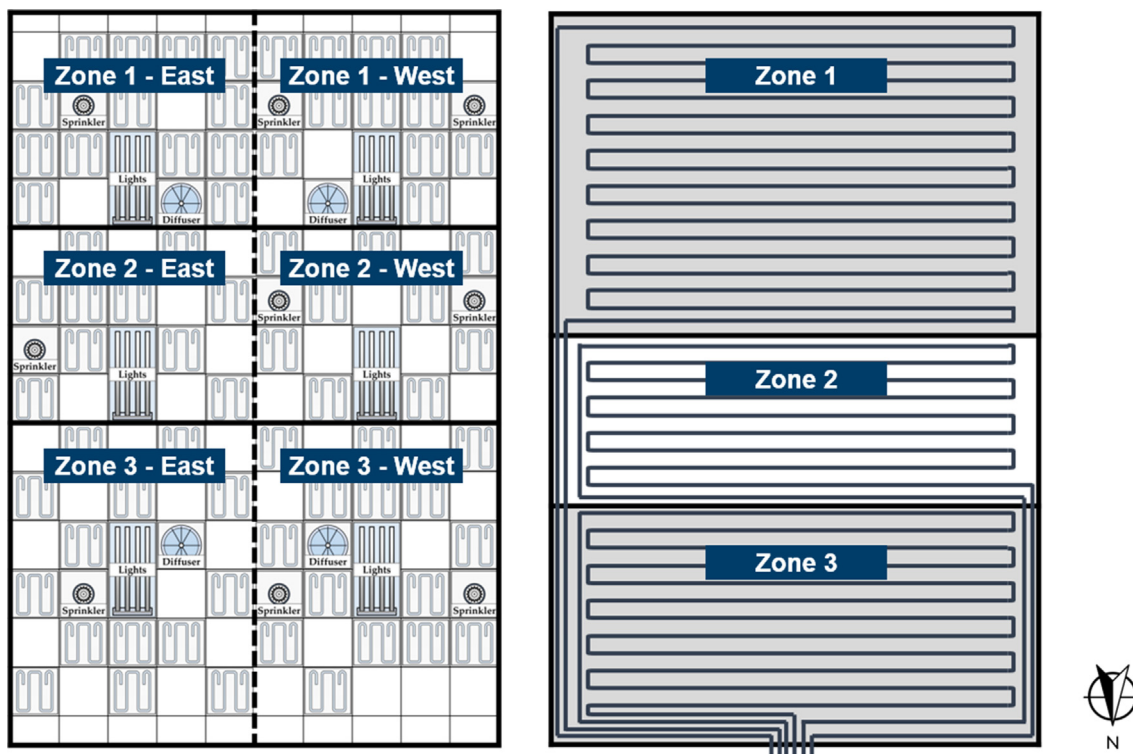


Fig. 5. Radiant system layout: RCP (left), radiant slab (right).

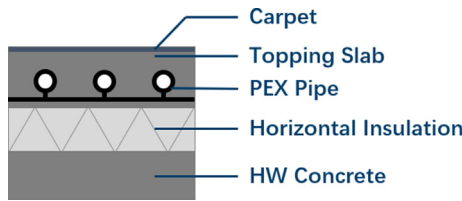


Fig. 6. The radiant slab system.

used, which were made by inserting Resistance Temperature Detector (RTD) sensors into table tennis balls coated with grey paint with an emissivity of ~ 0.90 . According to Benton [39], this type of globe thermometer has a response time of ~ 6 min to reach 90% of its final value.

The mean radiant temperature was calculated from the measured temperature of the globe, T_g , and the absolute dry-bulb temperature [20], as shown in Eq. (1).

$$T_r = \left[\frac{h_c}{\sigma\varepsilon} (T_g - T_a) + (T_g + 273.15)^4 \right]^{0.25} - 273.15 \quad (1)$$

For the globe temperature sensor used in this study, T_r was calculated using the following equation [39],

$$T_r = \left[\frac{6.32D^{-0.4}\nu^{0.5}}{\sigma\varepsilon} (T_g - T_a) + (T_g + 273.15)^4 \right]^{0.25} - 273.15 \quad (2)$$

As prescribed in ISO 7726 [20], in most practical cases where the relative speed is small (< 0.2 m/s) or where the difference between the mean radiant and air temperature is small (< 4 K), the operative temperature, T_{op} , can be approximated sufficiently accurately by the mean value of the mean radiant temperature, T_r , and the dry-bulb temperature, T_a .

The chilled water supply temperature was measured at the outlet of the buffer tank; the water temperatures at the inlet and outlet of each water circuit were also measured.

Outdoor dry-bulb and dew-point temperature and direct and diffuse

solar irradiance were measured on the roof of the adjacent double height test bed, the dry-bulb temperature sensor was housed in an aspirated enclosure and the dew point temperature was measured using a polished mirror sensor. Details of the sensors inside the test cell are presented in Table 4. All the sensors were sampled by the data acquisition system at an interval of one second and one-minute averages calculated for analysis purposes.

2.3. Experiment setup

Tests were conducted in March and April 2016 in Berkeley, California, which has a cool summer Mediterranean climate. The ASHRAE 1% design conditions for the nearby Oakland airport are 4.2 °C for heating and 25.4 °C dry bulb/17.8 °C mean coincident wet bulb for cooling. The choice of test period was based on two main considerations: (1) The south façade of the test cell has a high performance glazing system and the rest of the bounding surfaces are highly insulated, so the influence of the relative mild outside temperature is relatively modest; furthermore, Berkeley has similar ambient temperatures from March to July and so the test period is representative of summer time, and (2) Commercial buildings in temperate climates, for which radiant systems are particularly suitable, are typically cooling dominated year round. The solar elevation angle in March and April is intermediate between that in summer and in winter, making it more typical for assessing the impact of solar radiation on the thermal behavior of radiant systems. The cooling load is dominated by the solar gain and the internal gains, making the results applicable to south-facing spaces in commercial buildings with similar fenestration and internal gains over a range of climates defined in terms of ambient temperature. Ten test cases (5 for the RCP system and 5 for the RS system) were developed to cover a range of operational conditions to capture the characteristics of both systems, as shown in Table 5.

In the RCP system, the chilled water supply temperature was modulated between 13 °C and 20 °C to maintain the room operative temperature at the designated set-points based on the operation schedule. In the RS system, the chilled water was supplied to the slab based

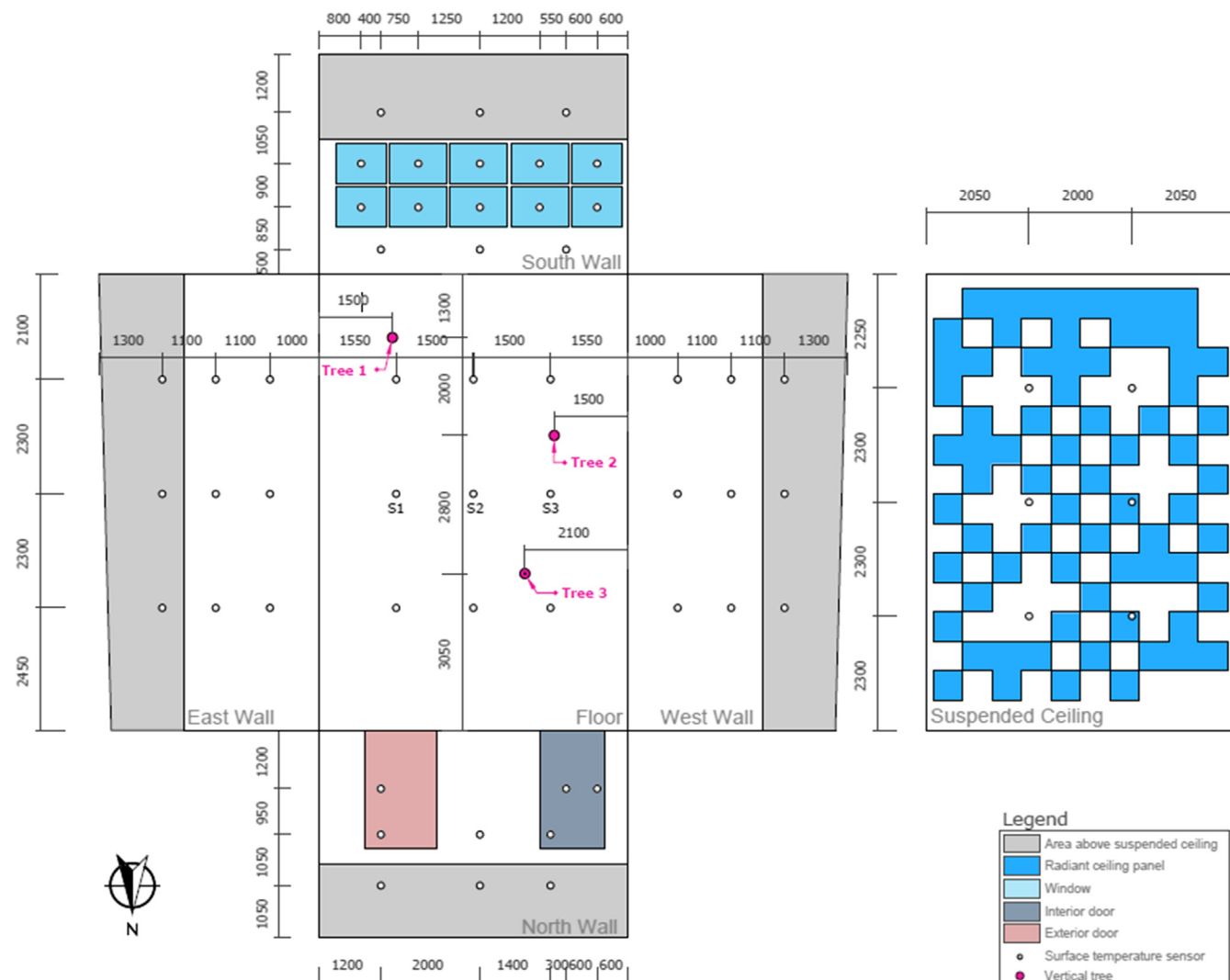


Fig. 7. Temperature sensor layout.



Fig. 8. The temperature measurements.

on the operation schedule as an open-loop control system.

In order to evaluate the effect of ceiling fans on air stratification, the ceiling fans were operated at different speeds at different times in Case 5 for the RCP system and Case 10 for the RS system. In Case 6, three carpet tiles were removed to expose the slab directly to the infrared (IR) camera. The IR images with both the exposed slab surface and the carpet were obtained to investigate the impact of the carpet on the floor

Table 3
Heights of the temperature sensors on the stratification tree.

Height above the floor (m)	Description
0.1	Ankle level
0.3	Knee level
0.6	Waist level for seated occupants
1.1	Head level for seated occupants
1.7	Head level for standing occupants
2.2	0.5 m below the drop ceiling
2.7	0.1 m below the drop ceiling

Table 4
Sensor specification.

Sensor type	Accuracy	Measurements
US Sensor PR103J2	± 0.05 K	Surface and air temperatures
RTD	± 0.03 K	Globe temperature
MAG 1100 PFA	± 0.41% at max flow rate	Water flow rate of each radiant circuit
BAPI RTD	± 0.03 K	Chilled water supply and return temperatures
BAPI XXP thermistor	± 0.05 K	Slab temperature
IR Camera	± 2 K	Carpet temperature

Table 5
Test cases.

Case	System type	Operation Schedule	$T_{oa,ave}$ (°C)	RH (%)	$Q_{solar,max}$ (W/m ²)	$T_{op,sp}$ (°C)	Q (L/s) ^a	$T_{w,sup}$ (°C)	Ceiling fan
1	RCP	00:00–24:00	13.7	72	885	23	0.303	13–20	Off
2	RCP	00:00–24:00	12.4	79	925	24	0.303	13–20	Off
3	RCP	00:00–24:00	14.7	72	890	25	0.303	13–20	Off
4	RCP	06:00–19:00	11.6	75	934	25	0.303	13–20	On
5	RCP	00:00–24:00	18.4	100	995	25	0.303	13–20	Off
6	RS	00:00–24:00	11.9	100	1000	N/A	0.303	13	Off
7	RS	00:00–24:00	11.9	100	279	N/A	0.152	13	Off
8	RS	00:00–24:00	10.8	100	393	N/A	0.303	15	Off
9	RS	00:00–24:00	12.4	100	1316	N/A	0.303	18	Off
10	RS	00:00–24:00	23.8	95	952	N/A	0.303	18	On

^a This is the total chilled water flow supplied to the radiant system, and it is distributed evenly to each circuit/sub-zone.

temperature and the cooling capacity.

3. Results and discussions

3.1. Stratification and effect of ceiling fans

Table 6 summarizes the results for the air stratification tests. Fig. 9 shows the vertical air temperature distributions for Cases 1–4, and each temperature value was averaged over the three positions shown in Fig. 7. ASHRAE [38] defines the temperature stratification as the vertical temperature difference between heights of 0.1 m and 1.7 m for a standing occupant, and 0.1 m and 1.1 m for a seated occupant, which correspond to the ankle and head heights for each case, and the maximum allowed temperature stratification is 3 K. As can be seen in Fig. 9, the maximum temperature stratification was 1.7 K occurred at 11:00 in Case 3 where the room operative temperature was controlled at 25 °C. As shown in Table 5, in Case 4, the RCP system ran only from 06:00 to 19:00, and was off during the night, as were the artificial lights. The resulting air temperature profile is significantly different from Cases 1–3. Almost same temperature was measured at all seven heights during the night. This indicates that not only solar, but also internal loads are the main drivers of stratification. Fig. 10 shows the results of the RS system, and the maximum temperature stratification was 3.0 °C occurred at 15:30 in Case 6, which is nearly twice as much as that in the RCP system. As shown in Figs. 9 and 10, the temperature stratifications in both the RCP and RS systems were noticeably smaller at night. In Cases 6–9, the RS system ran 24 h per day while all internal loads except the circulation pump were off at night. Despite different maximum stratification values, the temperature profiles showed a similar trend and the maximum stratification occurred during 15:00–17:00 in the RS system, while it varied significantly, and was highly dependent on test conditions, in the RCP system.

Table 6
Summary of air stratification.

System type	RCP					RS				
	1	2	3	4	5	6	7	8	9	10
$T_{oa,ave}$ (°C)	13.7	12.4	14.7	11.6	18.4	11.9	11.9	10.8	12.4	23.8
$Q_{solar,max}$ (W/m ²)	885	925	890	934	995	1000	279	393	1316	952
$T_{op,1.1,ave}$ (°C)	23.0	23.9	24.3	22.8	23.6	18.9	18.6	18.3	19.3	24.5
$T_{r,1.1,ave}$ (°C)	22.9	23.9	24.2	22.7	23.6	18.8	18.5	18.2	19.3	24.5
$T_{a,0.1,ave}$ (°C)	22.6	23.6	23.7	22.4	23.5	17.5	17.3	17.3	18.4	23.3
$T_{a,0.3,ave}$ (°C)	22.7	23.7	23.9	22.6	23.5	17.8	17.6	17.5	18.6	23.6
$T_{a,0.6,ave}$ (°C)	22.8	23.8	24.1	22.7	23.6	18.3	18.0	17.9	18.9	24.0
$T_{a,1.1,ave}$ (°C)	23.0	24.0	24.3	22.8	23.7	18.9	18.7	18.4	19.4	24.6
$T_{a,1.7,ave}$ (°C)	23.1	24.0	24.4	22.9	23.7	19.1	18.9	18.5	19.5	24.7
$T_{a,2.2,ave}$ (°C)	23.2	24.1	24.5	22.9	23.8	19.3	19.0	18.7	19.6	24.8
$T_{a,2.7,ave}$ (°C)	23.3	24.2	24.6	23.0	23.8	19.4	19.2	18.8	19.7	24.9
$\Delta T_{a,1.1-0.1,max}$ (K)	1.0	0.8	1.4	1.0	1.1	2.7	2.2	1.8	2.0	3.1
$\Delta T_{a,1.7-0.1,max}$ (K)	1.1	0.8	1.7	1.2	1.5	3.0	2.5	2.1	2.3	3.4

Fig. 11 shows the impact of ceiling fans on the performance of the RCP system. The three multi-speed ceiling fans were switched on at Level 2 from 10:20 to 15:00 and at Level 3 from 15:00 to 20:00. The maximum temperature stratification was 0.7 K when the fans were at Level 2, with an air speed of 1.1 m/s directly below the fan, and 0.4 K when the fans were at Level 3, with an air speed of 1.5 m/s (Case 5). Compared to Case 3, which had the ceiling fans off, the maximum temperature stratification in Case 5 was reduced by 1.0 K for Level 2 and 1.3 K for Level 3. It should be noted that the fluctuation of the air temperature from 10:20 to 10:30 in the bottom chart of Fig. 11 was caused by the researchers entering and exiting the test cell. Therefore, the maximum temperature stratification was determined after 11:00, when the room air had returned to equilibrium. It is also worth noting that the maximum air speed measured when the fans were at Level 3 exceeded the maximum air speed limit of 1.2 m/s specified in ASHRAE Standard 55. Even if it is necessary to restrict the fan speed to Level 2, or its equivalent in another product, the reduction in stratification from 1.7 K to 0.7 K is significant in increasing convective heat transfer to the ceiling panels, and is in addition to the main benefit of the fan in reducing thermal stress by increasing convective heat transfer from the occupants. Even without ceiling fan operation, the observed stratification is substantially less than the maximum stratification allowed in Standard 55, i.e. 3 K for seated occupants and 4 K for occupants who are standing.

Fig. 12 shows the impact of ceiling fans on temperature stratification in the RS system. The air in the room was well-mixed when the ceiling fans were turned on at Speed 3, with an average air speed of 1.5 m/s, in Case 10. There is a substantial reduction in the temperature stratification in the RS system, which improves the thermal comfort and enhances the heat transfer at the surface of the radiant slab.

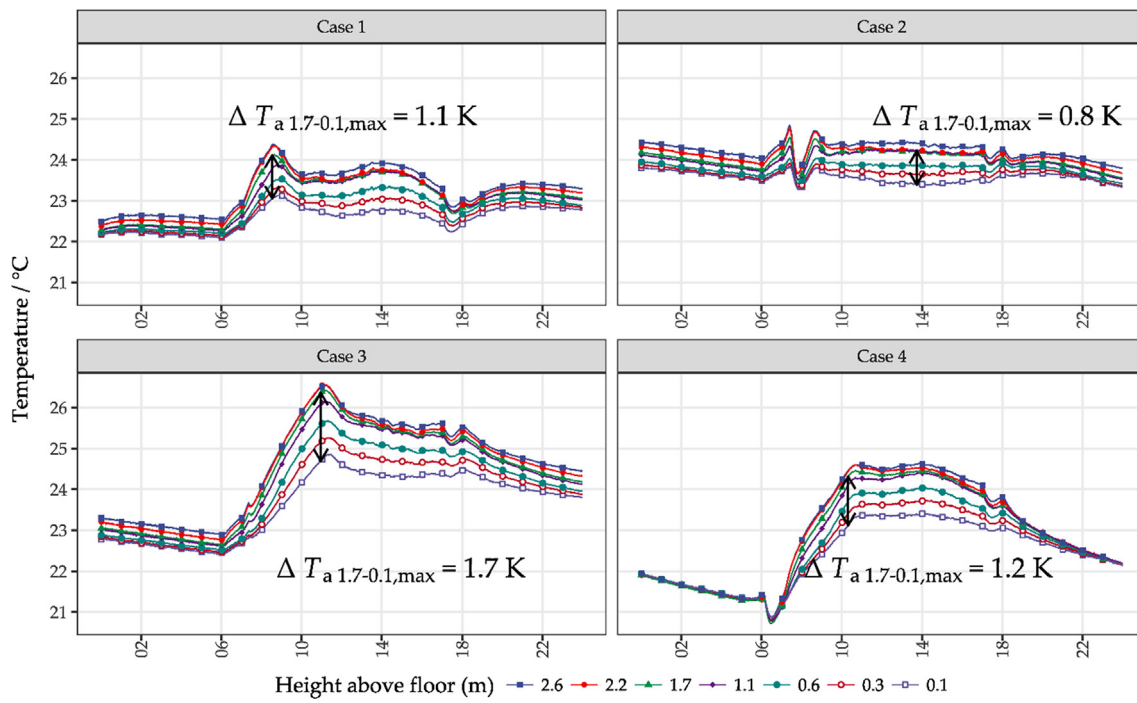


Fig. 9. Air temperature stratification in the RCP system.

3.2. Variation in comfort from perimeter to core

Fig. 13 shows the core-perimeter variations in dry-bulb temperature in the RCP system and the RS system, respectively. Each set of three lines represent the dry-bulb temperature vertical profiles at different locations (shown in Fig. 8). The steeper the slope of the lines, the less the variation in temperature with height. The larger the horizontal separations between the lines, the greater the dry-bulb temperature variations in going from the north end to the south end of the test cell. The larger horizontal separations in the left hand chart of Fig. 13

indicates that there are greater positional variations in temperature in the RCP system. The dependence of this effect on time of day, and the higher temperatures near the window, indicates the significant influence of solar radiation. The largest difference in temperature is between Tree 1 (near the south end) and Tree 3 (near the north end), with almost the same values for Cases 1–3. The largest variations for 1.1 m and 1.7 m were 1.1 K and 0.9 K respectively, occurred between 14:00 and 14:30.

The right chart in Fig. 13 shows the corresponding variations in dry-bulb temperature observed in the RS system. However, compared to the

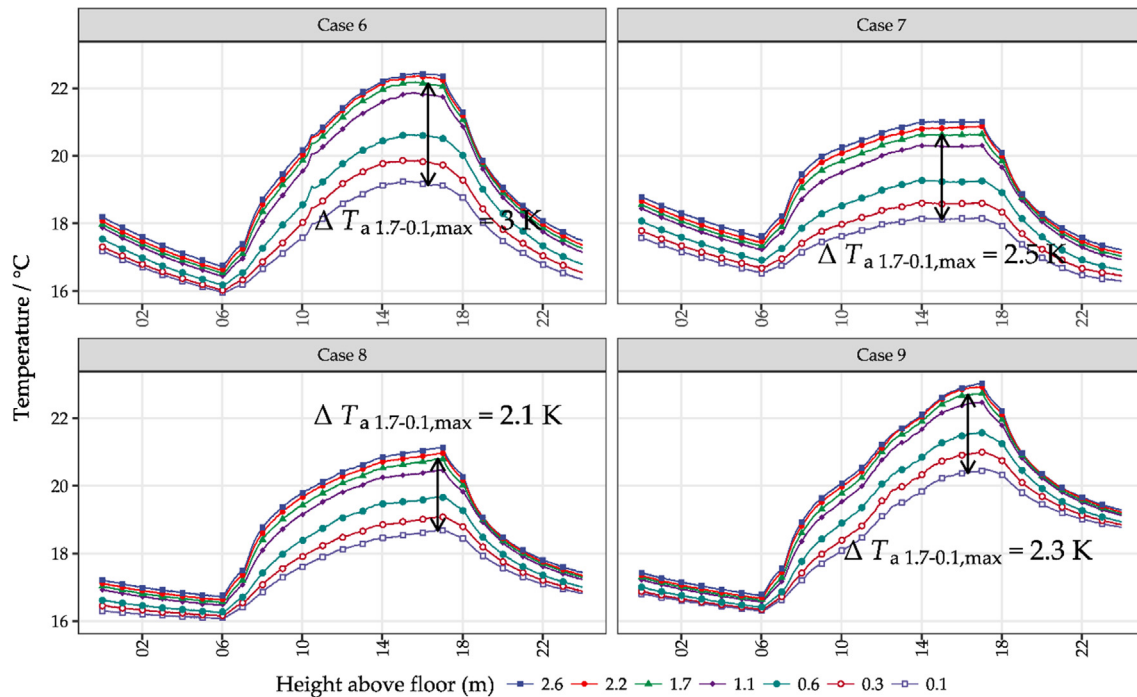


Fig. 10. Air temperature stratification in the RS system.

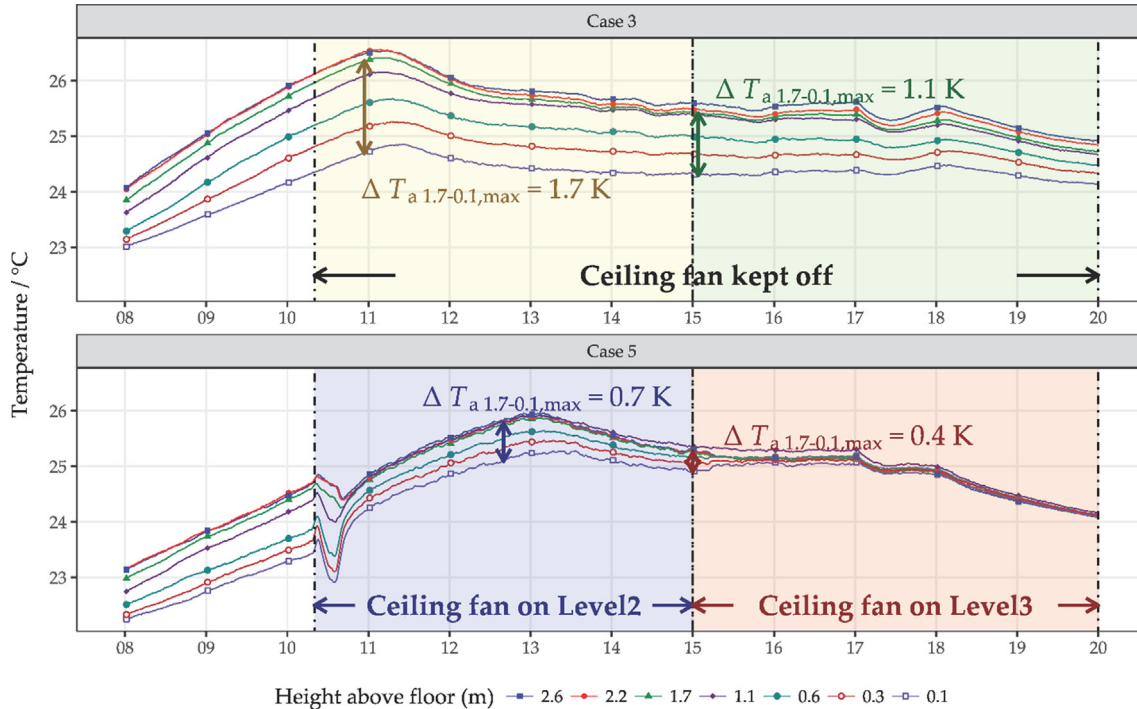


Fig. 11. The impact of ceiling fans on temperature stratification in the RCP system.

RCP system, the core-perimeter variation in the RS system was much smaller. Even though solar radiation still had a strong impact on the dry-bulb temperature in the space, the temperature differences between different locations had a relatively small maximum value of 0.6 K and 0.8 K for 1.1 m and 1.7 m respectively, occurring from 14:00 to 15:00. The reason for this difference in behavior is unclear, especially since the RS system produces stable stratification, which might be expected to inhibit horizontal mixing. One possible explanation is that the solar radiation impinging on the floor is removed directly by the radiant slab system, as reported previously [9,11], leaving the more uniformly-

distributed internal gains to drive the diurnal variation in room dry-bulb temperature.

3.3. Control on operative temperature vs. air temperature

Fig. 14 shows the difference between the spatially-averaged operative and dry-bulb air temperatures ($T_{op} - T_a$) for the RCP system on four test days. It can be seen that the difference between operative and air temperature is quite small, with a maximum value not exceeding 0.2 K. Between 9:00 and about 19:00, the operative temperature was

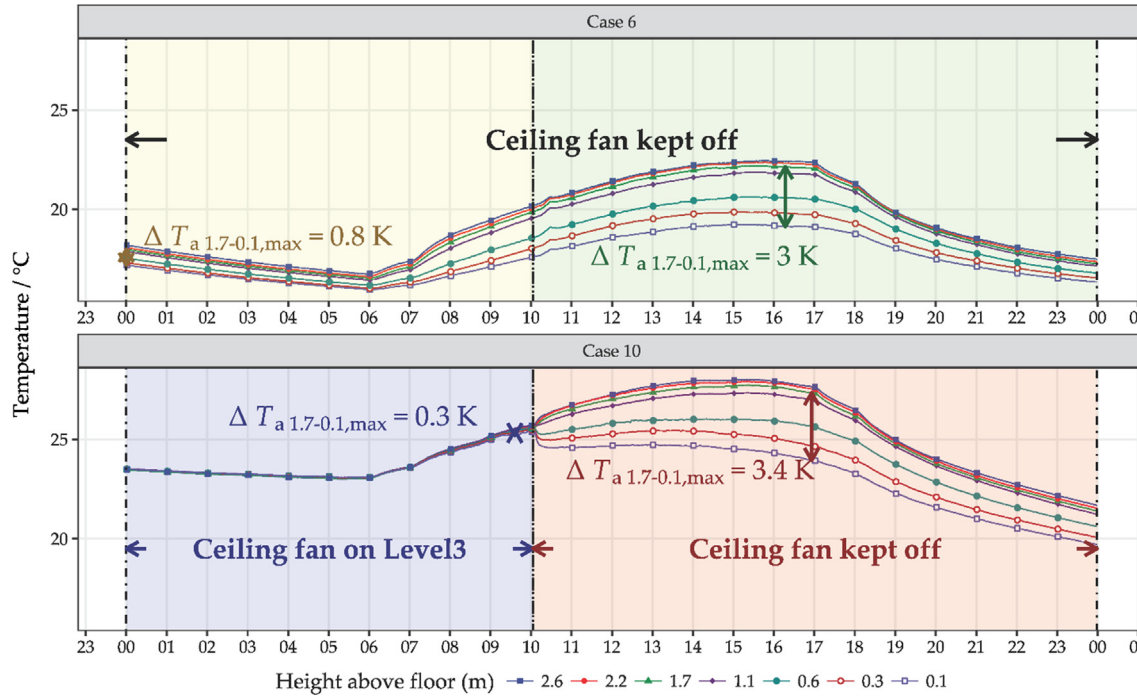


Fig. 12. The impact of ceiling fans on temperature stratification in the RS system.

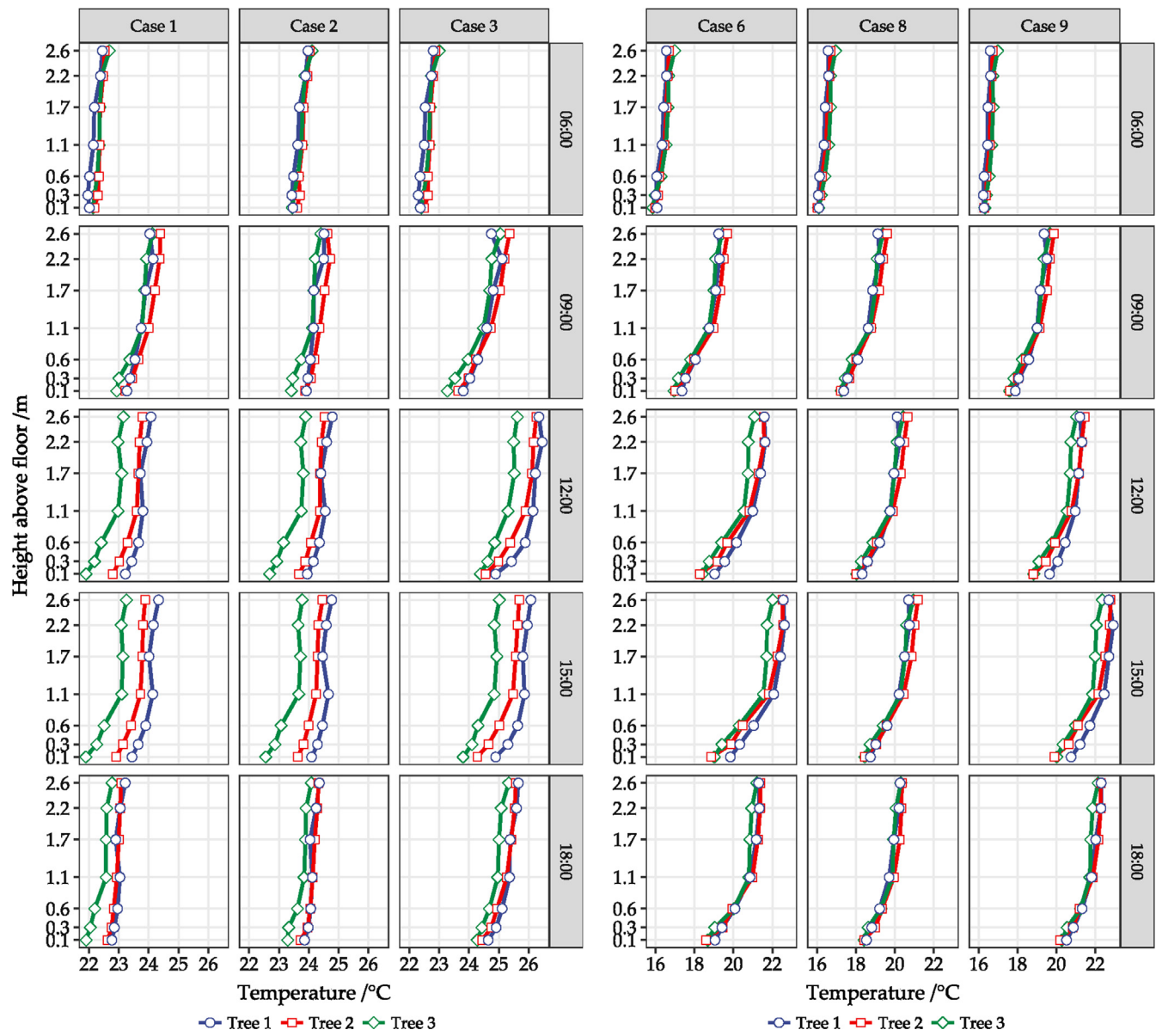


Fig. 13. Perimeter-core effect of room temperature in the RCP system (left) and the RS system (right).

higher than the air temperature and, for the rest of the day, it was lower than the air temperature. The pattern of profiles seems to be independent of the operative temperature set-point. This diurnal variation may be partly accounted for the surface temperature of the window being higher than the room air temperature during the day and lower than the room air temperature during the night. The small difference between the air temperature and the operative temperature indicates that it is possible to use air temperature instead of operative temperature for RCP cooling systems with relatively low loads that typically characterize radiant cooling systems. More work is required to investigate feasibility at higher cooling loads and for heating.

The motivation for controlling on air temperature instead of operative temperature is that conventional ‘thermostat’ air temperature sensors have lower first cost because they are produced on a larger scale and they have lower installation costs because they are more familiar to contractors. It is expected that this will remove one modest barrier to the adoption of RCP systems.

Fig. 15 shows the difference between the spatially-averaged operative and dry-bulb air temperatures ($T_{op} - T_a$) for the RS system on four test days. The difference is larger than in the case of the RCP

system, with a maximum value of 0.6 K. It should be noted that RS systems cannot be controlled with conventional feedback control strategies because of the long time constants involved. Model Predictive Control (MPC) [40], in which a simple model is used to predict the response to different control actions, or heuristic strategies informed by MPC, offer potential ways forward [41–43]. It is unclear whether the sensing of operative temperature, rather than air temperature, is required for acceptable performance of MPC.

3.4. Effect of carpet on cooling capacity

3.4.1. Temperature comparison using infrared thermography

The images shown in Fig. 16, which consist of infrared images superimposed on photographs of the measured surface, show the temperature distribution on the floor. There are two polygons, one enclosing an area of the slab surface without carpet and one enclosing a neighboring area with carpet. The maximum, average and minimum temperatures measured in each polygon are included in the figure. Three sites were measured. One was near the south wall where a sun patch may occur at noon; one was in the middle of the room; and one

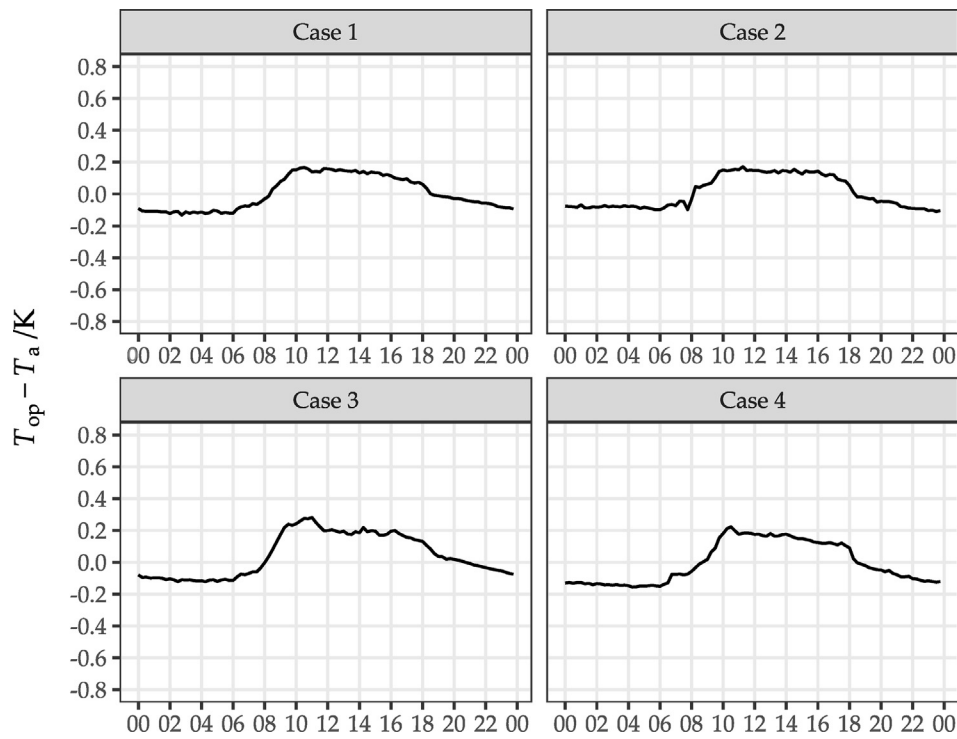


Fig. 14. The difference between the room operative temperature and the air temperature in the RCP system.

was near the north wall. Each site was measured twice. The site near the south wall showed a 1.0 K average temperature difference between the carpet and the exposed slab, while the other two sites showed smaller, similar differences, with 0.6 K at both the middle site and the north site. The small spikes in the middle of the IR images was due to the higher temperature of inset steel nuts used to secure temporary partitions.

3.4.2. Temperature comparison using temperature sensors

Nine temperature sensors were installed below the carpet as shown in Fig. 7. Fig. 17 shows the profiles of the three sensors S1, S2 and S3 in the middle of the room. The blue temperature line corresponds to sensor S1 with removed carpet tile, while the red and green lines correspond to sensors underneath carpet tiles. When the carpet tile above S1 was removed, at 13:00, the thermal resistance between the surface of the radiant slab and the other uncontrolled surfaces was reduced, which

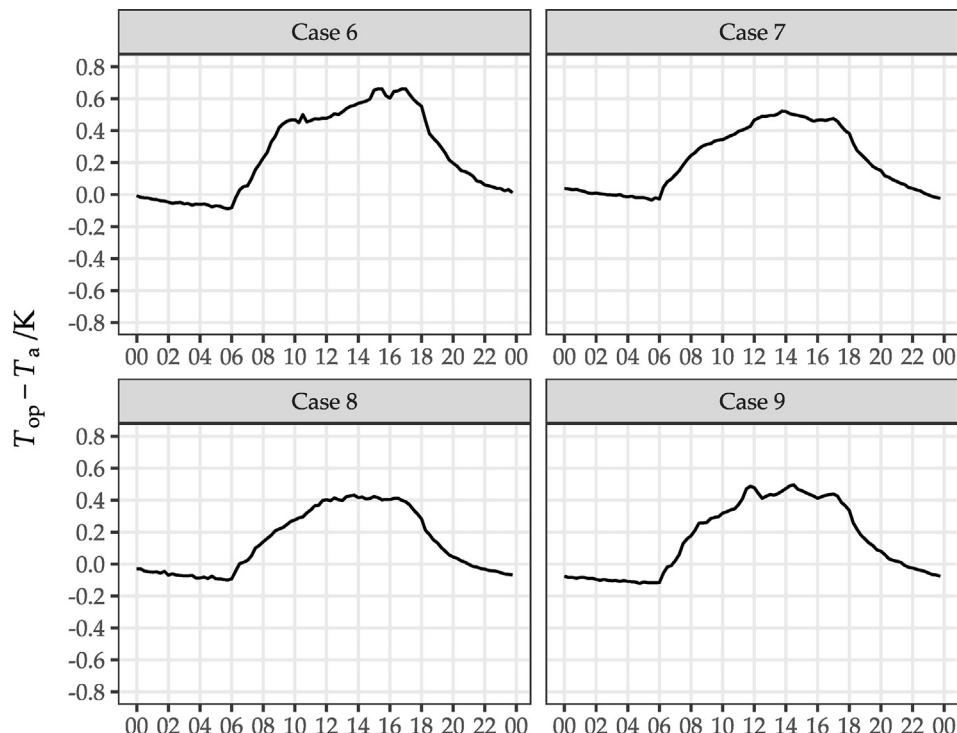


Fig. 15. The difference between the room operative temperature and the air temperature in the RS system.

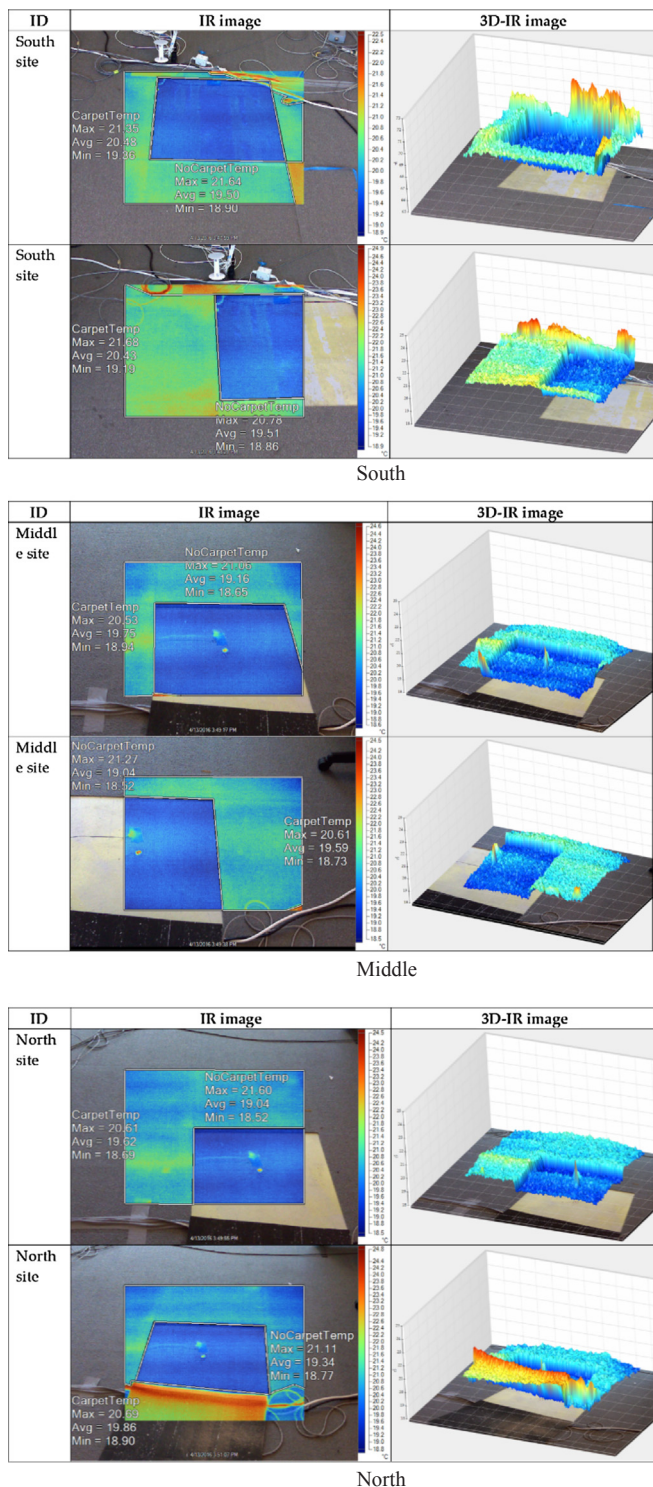


Fig. 16. Temperature distributions of the floor with and without carpet.

increased the radiant heat transfer between the slab and those surfaces, producing an increase in the surface temperature of the slab. Based on these measurements, use of carpet similar in thermal properties to that studied in this test would require the supply chilled water temperature to be reduced by 1.0 K, with a corresponding reduction in the opportunities for free cooling. A possible increase in condensation risk in the carpet and the pipes connecting the chilled water plant to the slab should be considered, along with (modest) changes to the design and control of any dedicated outdoor air system providing mechanically conditioned ventilation air.

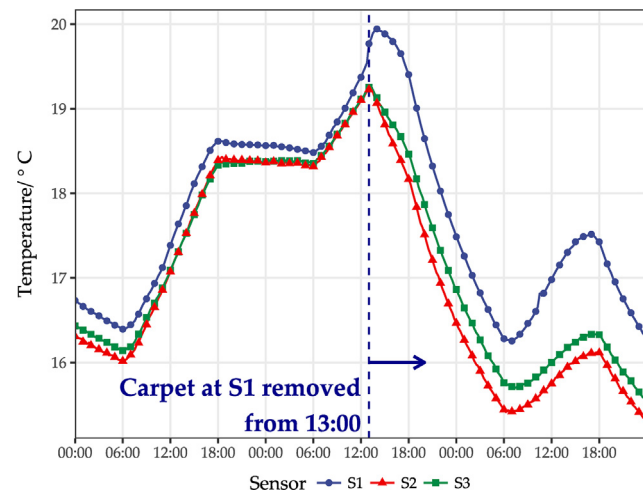


Fig. 17. The temperature profiles of the floor with and without carpet.

4. Conclusions

Both radiant ceiling panel (RCP) and radiant slab (RS) cooling systems can provide thermal comfort at the moderate zone cooling loads ($\sim 30 \text{ W/m}^2$ internal gains plus 40 W/m^2 solar gains = $\sim 70 \text{ W/m}^2$) typical of a south-facing perimeter zone in a reasonably well-designed office building, enabling low energy design based on water-side free cooling, in suitable climates. The primary results of the study are as follows:

1. In cooling mode, the air stratification effect was significantly greater in the RS system than in the RCP system. In the RCP system, the observed maximum stratification value is 1.7 K – too small to have a significant impact on thermal comfort [38], while in RS system, the value went up to 3.4 K between floor and standing head height, with a risk of exceeding the permitted limitation in ASHRAE Standard 55 [38]. Use of ceiling fans would serve to reduce any excess stratification and/or provide thermal comfort at higher zone temperatures.
2. In both the RCP and RS systems, there is no need to incur the additional expense of a separate control zone at the perimeter of a 50% window-to-wall ratio unshaded south façade. The elevation of zone dry-bulb temperature near the south façade was primarily driven by the solar radiation. The peak value usually occurs approximately three hours after solar noon, the time lag being due to the thermal capacity of the floor. Again, this effect is too small to have a significant impact on thermal comfort.
3. Modest variations in comfort conditions were observed near unshaded south-facing windows. These variations could be mitigated by interior or exterior shading or by ceiling fans, without needing separate hydronic loops and controls, thus avoiding increased design, installation and maintenance costs.
4. In the RCP system, the difference between the operative temperature and air temperature is quite small if the loads can be met by the RCP system ($\leq 30 \text{ W/m}^2$). The observed difference did not exceed 0.2 K in cooling mode. This makes it possible to use air temperature as the controlled variable input to the zone temperature controller instead of the operative temperature, with significant cost savings. The difference for the RS system is larger than in the case of the RCP system, with a maximum value of 0.6 K.
5. In the RS system, the use of thin carpet requires the supply chilled water temperature to be reduced by ~ 1.0 K, with a corresponding reduction in the opportunities for free cooling and an increase in condensation risk.

Acknowledgement

The authors wish to thank Darryl Dickerhoff, Christian Fitting, Daniel Fuller, Christoph Gehbauer, Howdy Goudey, Ari Harding, Nicholas Lofgren, Brijesh Pandey, Shoba Varma, and Cynthia Regnier for technical support.

This study was funded by Pacific Gas and Electric Company's Emerging Technology – Technology Introductory Support program under internal project number ET14PGE8581 and was supported, in part, by the Assistant Secretary for Energy Efficiency and Renewable Energy, Office of Building Technology, State and Community Programs of the U.S. Department of Energy under Contract No. DE-AC02-05CH11231.

References

- [1] Kim KW, Olesen BW. Part one: radiant heating and cooling systems. *ASHRAE J* 2015;57:28.
- [2] Kim KW, Olesen BW. Part two: radiant heating and cooling systems. *ASHRAE J* 2015;57:34.
- [3] Olesen BW. Radiant floor heating in theory and practice. *ASHRAE J* 2002;44:19–26.
- [4] ISO. ISO 11855-2:2012(E): Building environment design – Design, dimensioning, installation and control of embedded radiant heating and cooling systems – Part 2: determination of the design heating and cooling capacity; 2012.
- [5] Gwerder M, Lehmann B, Tödtli J, Dorer V, Renggli F. Control of thermally-activated building systems (TABS). *Appl Energy* 2008;85:565–81. <http://dx.doi.org/10.1016/j.apenergy.2007.08.001>.
- [6] Gwerder M, Tödtli J, Lehmann B, Dorer V, Güntensperger W, Renggli F. Control of thermally activated building systems (TABS) in intermittent operation with pulse width modulation. *Appl Energy*. 2009;86:1606–16. <http://dx.doi.org/10.1016/j.apenergy.2009.01.008>.
- [7] Rhee K-N, Kim KW. A 50 year review of basic and applied research in radiant heating and cooling systems for the built environment. *Build Environ* 2015;91:166–90. <http://dx.doi.org/10.1016/j.buildenv.2015.03.040>.
- [8] Karmann C, Schiavon S, Bauman F. Thermal comfort in buildings using radiant vs. all-air systems: a critical literature review. *Build Environ* 2017;111:123–31. <http://dx.doi.org/10.1016/j.buildenv.2016.10.020>.
- [9] (Dove) Feng J, Schiavon S, Bauman F. Cooling load differences between radiant and air systems. *Energy Build* 2013;65:310–21. <http://dx.doi.org/10.1016/j.enbuild.2013.06.009>.
- [10] Bauman F, Feng J, Schiavon S. Cooling load calculations for radiant systems are they the same traditional methods. *ASHRAE J* 2013.
- [11] Feng J, Schiavon S, Bauman F. Comparison of zone cooling load for radiant and all-air conditioning systems. *Cent Built Environ* 2012<http://www.escholarship.org/uc/item/9g24f38j>.
- [12] Causone F, Corgnati SP, Filippi M, Olesen BW. Solar radiation and cooling load calculation for radiant systems: definition and evaluation of the Direct Solar Load. *Energy Build* 2010;42:305–14. <http://dx.doi.org/10.1016/j.enbuild.2009.09.008>.
- [13] Causone F, Corgnati SP, Filippi M, Olesen BW. Experimental evaluation of heat transfer coefficients between radiant ceiling and room. *Energy Build* 2009;41:622–8. <http://dx.doi.org/10.1016/j.enbuild.2009.01.004>.
- [14] Imanari T, Omori T, Bogaki K. Thermal comfort and energy consumption of the radiant ceiling panel system. *Energy Build* 1999;30:167–75. [http://dx.doi.org/10.1016/S0378-7788\(98\)00084-X](http://dx.doi.org/10.1016/S0378-7788(98)00084-X).
- [15] Song D, Kim T, Song S, Hwang S, Leigh S-B. Performance evaluation of a radiant floor cooling system integrated with dehumidified ventilation. *Appl Therm Eng* 2008;28:1299–311. <http://dx.doi.org/10.1016/j.applthermaleng.2007.10.020>.
- [16] Causone F, Baldin F, Olesen BW, Corgnati SP. Floor heating and cooling combined with displacement ventilation: possibilities and limitations. *Energy Build* 2010;42:2338–52. <http://dx.doi.org/10.1016/j.enbuild.2010.08.001>.
- [17] Schiavon S, Bauman F, Tully B, Rimmer J. Room air stratification in combined chilled ceiling and displacement ventilation systems. *HVACR Res* 2012;18:147–59.
- [18] Zhao M, Gu ZL, Kang WB, Liu X, Zhang LY, Jin LW, Zhang QL. Experimental investigation and feasibility analysis on a capillary radiant heating system based on solar and air source heat pump dual heat source. *Appl Energy* 2017;185(Part 2):2094–105. <http://dx.doi.org/10.1016/j.apenergy.2016.02.043>.
- [19] ISO. ISO 11855-1:2012(E): Building environment design – Design, dimensioning, installation and control of embedded radiant heating and cooling systems – part 1: definition, symbols, and comfort criteria; 2012.
- [20] ISO. ISO 7726-1998: Ergonomics of the thermal environment, instruments for measuring physical quantities; 1998.
- [21] American Society of Heating, Ventilating, and Air Conditioning Engineers. ASHRAE Handbook 2009 – Fundamentals. Atlanta; 2009.
- [22] Halawa E, van Hoof J, Soebarto V. The impacts of the thermal radiation field on thermal comfort, energy consumption and control—a critical overview. *Renew Sustain Energy Rev* 2014;37:907–18. <http://dx.doi.org/10.1016/j.rser.2014.05.040>.
- [23] Karmann C, Bauman FS, Raftery P, Schiavon S, Frantz WH, Roy KP. Cooling capacity and acoustic performance of radiant slab systems with free-hanging acoustical clouds. *Energy Build* 2017;138:676–86.
- [24] Bessoudo M, Tzempelikos A, Athienitis AK, Zmeureanu R. Indoor thermal environmental conditions near glazed facades with shading devices – Part I: experiments and building thermal model. *Build Environ* 2010;45:2506–16. <http://dx.doi.org/10.1016/j.buildenv.2010.05.013>.
- [25] Tzempelikos A, Bessoudo M, Athienitis AK, Zmeureanu R. Indoor thermal environmental conditions near glazed facades with shading devices – Part II: thermal comfort simulation and impact of glazing and shading properties. *Build Environ* 2010;45:2517–25. <http://dx.doi.org/10.1016/j.buildenv.2010.05.014>.
- [26] Gan G. Analysis of mean radiant temperature and thermal comfort. *Build Serv Eng Res Technol* 2001;22:95–101. <http://dx.doi.org/10.1191/014362401701524154>.
- [27] Tzempelikos A, Athienitis AK. The impact of shading design and control on building cooling and lighting demand. *Sol Energy* 2007;81:369–82. <http://dx.doi.org/10.1016/j.solener.2006.06.015>.
- [28] Feng J. Design and control of hydronic radiant cooling systems, University of California, Berkeley, CA – Doctor of Philosophy; 2014.
- [29] Bauman F, Webster T, Dickerhoff D, Schiavon S, Feng D, Basu C. Case study report: David Brower Center; 2011. <https://escholarship.org/uc/item/7tc0421f> [accessed March 5, 2018].
- [30] Lehmann B, Dorer V, Gwerder M, Renggli F, Tödtli J. Thermally activated building systems (TABS): Energy efficiency as a function of control strategy, hydronic circuit topology and (cold) generation system. *Appl Energy* 2011;88:180–91. <http://dx.doi.org/10.1016/j.apenergy.2010.08.010>.
- [31] Jin X, Zhang X, Luo Y, Cao R. Numerical simulation of radiant floor cooling system: the effects of thermal resistance of pipe and water velocity on the performance. *Build Environ* 2010;45:2545–52. <http://dx.doi.org/10.1016/j.buildenv.2010.05.016>.
- [32] Zhou G, He J. Thermal performance of a radiant floor heating system with different heat storage materials and heating pipes. *Appl Energy* 2015;138:648–60. <http://dx.doi.org/10.1016/j.apenergy.2014.10.058>.
- [33] Šíroky J, Oldewurtel F, Cigler J, Prívara S. Experimental analysis of model predictive control for an energy efficient building heating system. *Appl Energy* 2011;88:3079–87. <http://dx.doi.org/10.1016/j.apenergy.2011.03.009>.
- [34] Zhao K, Liu X-H, Jiang Y. Application of radiant floor cooling in large space buildings – a review. *Renew Sustain Energy Rev* 2016;55:1083–96. <http://dx.doi.org/10.1016/j.rser.2015.11.028>.
- [35] Lawrence Berkeley National Laboratory, FLEXLAB; 2016. <https://flexlab.lbl.gov/> [accessed December 22, 2016].
- [36] California Energy Commission. Building Energy Efficiency Standards For Residential And Nonresidential Buildings; 2012. <http://134.186.116.98/2012publications/CEC-400-2012-005/CEC-400-2012-005-CMF-REV3.pdf> [accessed January 29, 2017].
- [37] European Committee for Standardization. EN 14240-2004: Ventilation for buildings—chilled ceilings—testing and rating; 2004.
- [38] ASHRAE. ANSI/ASHRAE Standard 55-2013: Thermal environmental conditions for human occupancy; 2013.
- [39] Benton C, Bauman F, Fountain M. A field measurement system for the study of thermal comfort. *ASHRAE Trans* 1990;96:12.
- [40] Afram A, Janabi-Sharifi F. Theory and applications of HVAC control systems – a review of model predictive control (MPC). *Build Environ* 2014;72:343–55. <http://dx.doi.org/10.1016/j.buildenv.2013.11.016>.
- [41] Lim J-H, Song J-H, Song S-Y. Development of operational guidelines for thermally activated building system according to heating and cooling load characteristics. *Appl Energy* 2014;126:123–35. <http://dx.doi.org/10.1016/j.apenergy.2014.03.087>.
- [42] Schmelas M, Feldmann T, Bollin E. Savings through the use of adaptive predictive control of thermo-active building systems (TABS): a case study. *Appl Energy* 2017;199:294–309. <http://dx.doi.org/10.1016/j.apenergy.2017.05.032>.
- [43] Bianchini G, Casini M, Vicino A, Zarrilli D. Demand-response in building heating systems: a model predictive control approach. *Appl Energy* 2016;168:159–70. <http://dx.doi.org/10.1016/j.apenergy.2016.01.088>.